Kinetics of decomposition in ionic solids: II. Neutron scattering study of the system AgCl-NaCl



2001 J. Phys.: Condens. Matter 13 11521

(http://iopscience.iop.org/0953-8984/13/50/311)

INSTITUTE OF PHYSICS PUBLISHING JOURNAL OF PHYSICS: CONDENSED MATTER

J. Phys.: Condens. Matter **13** (2001) 11521–11530 PII: S0953-8984(01)27914-4

# Kinetics of decomposition in ionic solids: II. Neutron scattering study of the system AgCl–NaCl

**D Caspary[1], G Eckold[1], F Güthoff[1] and W Pyckhout-Hintzen[2]**

[1] Institut für Physikalische Chemie and Sonderforschungsbereich 345, Universität Göttingen, Tammannstrasse 6, D-37077 Göttingen, Germany
[2] Institut für Festkörperforschung, Forschungszentrum Jülich, D-52425 Jülich, Germany

Received 15 August 2001, in final form 11 October 2001
Published 30 November 2001
Online at stacks.iop.org/JPhysCM/13/11521

**Abstract**

The kinetic of decomposition in the quasi-binary ionic system AgCl–NaCl has been studied by means of time-resolved neutron diffraction and small-angle neutron scattering. The coherent critical point is estimated as 447 ± 3 K, 24 K below the upper critical binodal temperature. The chemical decomposition is almost completed in the first 200 s irrespective of the temperature. The mechanical relaxation of the lattice, however, takes place on a much longer timescale and is dominated by coherency strains leading to metastable intermediate states.

## 1. Introduction

Mixed ionic systems of the silver alkali halide type provide almost ideal systems for the investigation of decomposition processes. Simple lattice structures, the absence of structural phase transitions, the large ionic mobility of cations and an almost rigid framework of the halide sublattice make these systems suitable for real-time kinetic studies. The observation of transient states during the demixing process provides valuable information about the underlying microscopic mechanism.

In a first paper on the system AgBr–NaBr [1] it was shown that coherency strains due to the lattice parameter mismatch of the pure compounds play an important role. It was demonstrable that the characteristic features of spinodal decomposition are observable by means of small-angle neutron scattering (SANS) if the sample is quenched into the unstable regime of the phase diagram. Here, the phase separation is governed by concentration fluctuations of small amplitudes and large wavelengths. Due to mechanical strains, the spinodal is suppressed with respect to the binodal by about 100 K and, hence, there is a rather large metastable regime where the decomposition is driven by nucleation-and-growth processes. It is the combination of SANS and diffraction which provides a consistent idea of the decomposition process. As shown in [1], the chemical decomposition takes place on a rather short timescale of some 100 s while the mechanical relaxation of the lattice needs a much longer period of time.

  

The influence of coherency strains can be studied in a systematic way by changing the constituents: while the lattice parameter mismatch in the AgBr–NaBr system is about 3.4%, it is reduced by about a factor of two on moving to the chloride system AgCl–NaCl. Hence, according to Cahn [2], the suppression of the spinodal is expected to be about a factor of four smaller than in the bromide system (see also equation (4) below). Since the demixing process is almost completely confined to the cation subsystem, the replacement of bromide by chloride ions just changes the framework for the rearrangement of silver and sodium ions.

There are very few investigations in the literature [3–5] which provide a rough estimate for the timescale of decomposition. However, no quantitative information exists about the temperature-dependent evolution of the morphology of precipitates (as reflected by small-angle scattering) and the evolution of the lattice structure (as reflected by diffraction). In the present paper, we therefore report on time-resolved experiments using SANS and diffraction in the fluctuation regime below the spinodal.

The AgCl–NaCl phase diagram as determined by Sinistri *et al* [6] exhibits an almost symmetrical miscibility gap with a critical temperature $T_{\mathrm{crit}} \approx 471$ K and a critical concentration $x_{\mathrm{crit}} \approx 0.497$. (Note that throughout this paper concentrations are always given in mole fractions of AgCl.) Due to the smaller lattice parameter mismatch, $T_{\mathrm{crit}}$ is considerably smaller than in the bromide system ($T_{\mathrm{crit}} \approx 558$ K). Interestingly, sodium chloride exhibits a larger lattice parameter than silver chloride (0.5633 nm as compared to 0.5539 nm for AgCl at ambient temperature), although the ionic radius of sodium is larger than that of silver. This effect seems to be a direct consequence of the large polarizability of silver ions.

## 2. Experimental procedure

To prepare the AgCl–NaCl samples, the pure salts (AgCl Merck and Acros 99.5%, NaCl Merck 99.5%) were ground to small pieces in a mortar. The equimolar mixture ($x = 0.5$) was heated in a $N_2$ atmosphere at 773 K to dissolve the NaCl in liquid AgCl. Subsequently, after solidification and cooling to room temperature, the product was ground to a grain size less than 0.040 mm. The powder was pressed into polycrystalline pellets of 40 mm diameter and 5 mm thickness for the diffraction experiments and pellets of 20 mm diameter and about 1.5 mm thickness for the SANS experiments. Wrapped in silver foil, the pellets were annealed at 673 K for 6 h to guarantee homogeneity. The temperature was determined by NiCr–Ni thermocouples and the accuracy of the absolute temperature was, in all experiments, $\pm 3$ K.

The SANS experiments were performed using the KWS-1 instrument at the FRJ-2 reactor in Jülich. After the quench of the sample at a rate of about 10 K $s^{-1}$ from 673 K to different temperatures below $T_{\mathrm{crit}} \approx 471$ K, the scattered intensity was measured sequentially as a function of time. The time steps between two successive data sets was 60 s in most experiments. Additional runs with time channels of 30 and 120 s were also performed. The neutron wavelength was chosen as 0.7 nm. The sample–detector distances of 4 and 8 m yield an accessible wave-vector-transfer range of 0.1–0.8 and 0.05–0.4 $nm^{-1}$, respectively. In the usual manner, the scattered intensity was corrected for background and detector efficiency and calibrated using a high-density polyethylene (Lupolen) sample. After taking the radial average, the reference data for the homogeneous phase at $T = 673$ K were subtracted.

The diffraction experiments were performed at the UNIDAS triple-axis spectrometer in Jülich using 0.236 nm neutrons. Most of the data were taken at the (2 0 0) Bragg reflection using the tight collimation of 0.25° corresponding to a linewidth of 0.011 r.l.u. (FWHM). Unlike the SANS experiments, which were performed sequentially in time, the diffraction experiments were carried out using the stroboscopic technique [7] which allows one to achieve an adequate time resolution even with a single detector. During these experiments, the temperature was

cycled between the homogenization and the decomposition temperature by rapid heating and cooling. The scattered intensity for each single scan-point was registered as a function of time and accumulated over several cycles. The results are perfectly reproducible and do not depend on the history of the sample. Hence, identical states are passed through during each individual cycle. Due to the larger sample, the quench rate was reduced to about 2 K $s^{-1}$ which, however, does not affect the results, as shown below. Adapted to the time resolution of the SANS experiments, the width of the individual time channels was chosen to be 60 s.

It should be noted that for all experiments the zero point of the timescale ($t = 0$) is chosen as the moment when the ageing temperature is actually reached.

## 3. Results

### *3.1. Small-angle neutron scattering*

Within the time range of the present experiments, significant small-angle scattering intensity could only be detected below temperatures of about 450 K. A representative example of the time evolution of the scattering profile is shown in figure 1 for a decomposition temperature of 373 K. There is a pronounced correlation peak in the scattered intensity around $Q_{\max} \approx 0.2$ $nm^{-1}$ which is characteristic for spinodal decomposition. The experimental data can quantitatively be described by Furukawa's phenomenological *ansatz* [8]:

$$\frac{d\Sigma}{d\Omega}(Q) = \frac{d\Sigma}{d\Omega}(Q_{\max}) \left(1 + \frac{\beta}{\gamma}\right) \frac{\left(Q/Q_{\max}\right)^{\gamma}}{\beta/\gamma + \left(Q/Q_{\max}\right)^{\beta+\gamma}}. \tag{1}$$

In fact, the solid curves in figure 1 are fits to this function. The exponents $\beta$ and $\gamma$ characterize the asymptotic behaviour for $Q \to \infty$ and for $Q \to 0$, respectively. The fits of our data yield values of about $\beta \approx 6.0$ and $\gamma \approx 3.5$ for the early stages and $\beta \approx 4.5$ and $\gamma \approx 2.5$ for the late stages, respectively. Moreover, we recognize that the position $Q_{\max}$ of the correlation peak is shifted towards zero during decomposition. Finally, for very long times the correlation peak disappears and the scattering profiles may be described by Porod's law [9] with $d\Sigma/d\Omega(Q) \propto Q^{-4}$ in the accessible $Q$-range. This finding indicates that the final morphology of the system is dominated by well defined precipitates with sharp interfaces.

The time dependence of $Q_{\max}$ is shown in figure 2. Obviously, there is a continuous decrease of $Q_{\max}$ even for small $t$. Consequently, the correlation length $2\pi/Q_{\max}$, which is the dominant wavelength of the composition fluctuations, increases with time. After half an hour the characteristic length scale reaches 33 nm at 373 K, 42 nm at 393 K and 60 nm at 433 K. At all temperatures, $Q_{\max}$ is found to be almost proportional to $t^{-1/3}$. According to Lifshitz and Slyozov [10] this behaviour is expected for diffusion-controlled coarse graining.

These late states of decomposition processes are usually described by scaling theories [11–16] which take into account the self-similar evolution of decomposition patterns. As a result, the intensity profiles for a three-dimensional system can be represented by a time-independent master curve which is obtained by plotting $Q_{\max}^3 \, d\Sigma/d\Omega$ versus $Q/Q_{\max}$. Figure 3 displays the corresponding data for selected time steps at 373 K within the early (top) and late (bottom) stages of decomposition. While in the earlier stages up to 2000 s there is a considerable variation in the individual profiles, the scaling behaviour is rather well followed after about 2500 s.

The integrated intensity can be used to characterize the kinetics of the decomposition process. From the experimental data, integrated intensities were calculated via the fit to the Furukawa function, equation (1), thus providing a reasonable extrapolation to large $Q$-values. The corresponding time evolution in shown in figure 4. Obviously, the intensity increases almost instantaneously up to a saturation value which is temperature dependent.

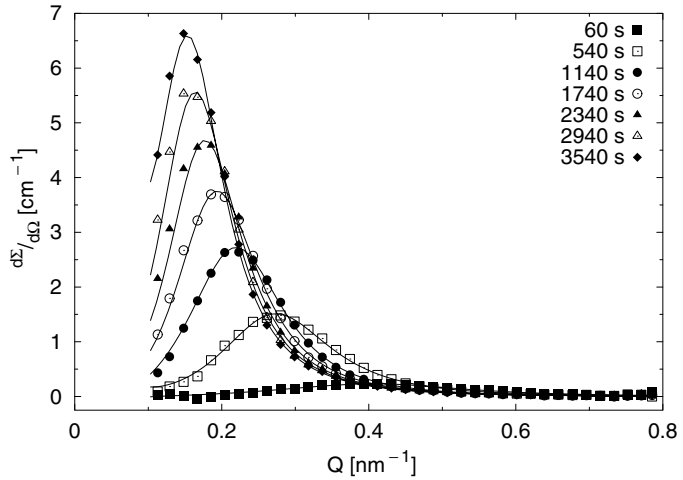


**Figure 1.** Time evolution of the small-angle intensity at 373 K. The solid curves are the results of fits to the Furukawa function (equation (1)).

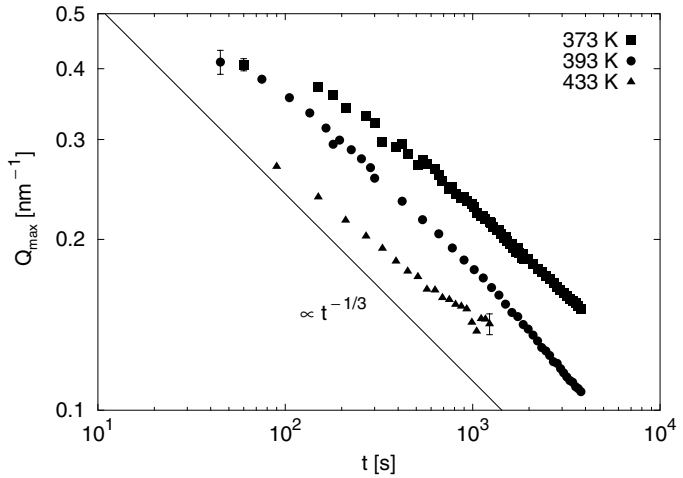


**Figure 2.** The time dependence of the position $Q_{max}$ of the correlation peak.

With decreasing temperature the small-angle intensity grows in accordance with the increasing width of the miscibility gap. Hence, it is concluded that this jump of the intensity is due to chemical demixing which takes place within some 100 s. On a much longer timescale of several thousand seconds, another slight increase of the intensity is observed.

### *3.2. Neutron diffraction*

The behaviour of the crystal lattice during decomposition may be characterized by the changes of the profiles of Bragg reflections due to the lattice parameter mismatch of the product phases. As a typical example, the time evolution of the (200) reflection at 373 K is shown in figure 5. At $t = 90$ s, the Bragg peak is a sharp line, the width being determined by experimental resolution. Even after 1590 s, when the small-angle intensity has already reached its saturation

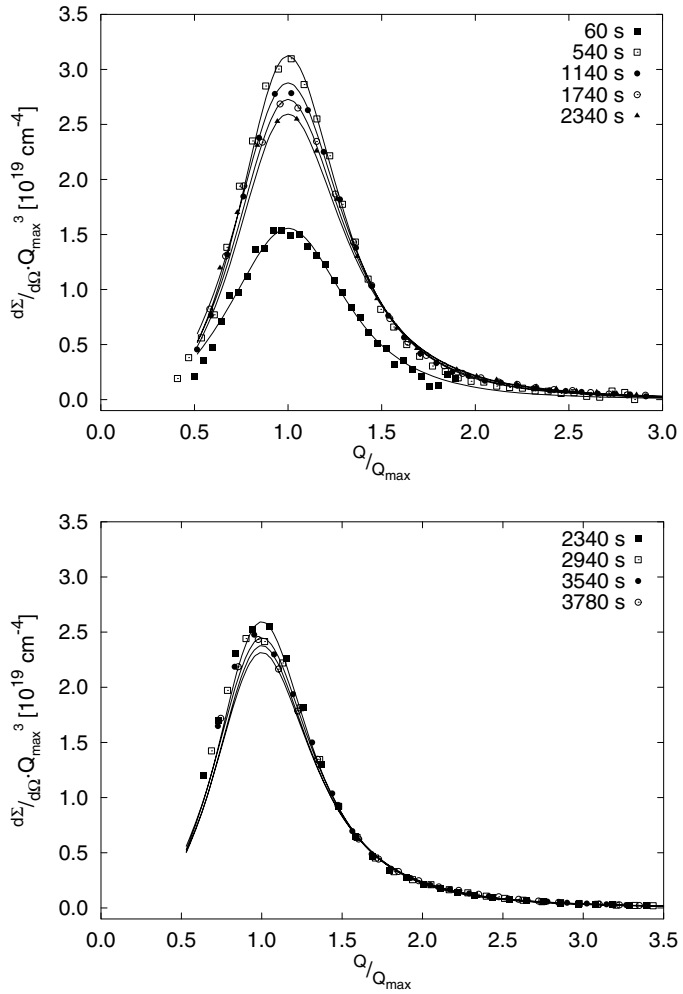


**Figure 3.** The scaling behaviour of the small-angle intensity at early stages (top) and late stages (bottom), both at 373 K. The solid curves are the results of fits using the Furukawa function (equation (1)).

value (cf figure 4), the shape of the central line is conserved. In particular, there is no indication of a splitting of the lattice parameters: the two arrows in figure 5 label the positions where the Bragg peaks of the two equilibrium phases with the binodal concentrations would be expected. Obviously, the lattice is not changed even though the phase separation has taken place.

Careful inspection of the diffraction data yields, however, that at $Q \approx 1.98$ r.l.u. and $Q \approx 2.02$ r.l.u. additional intensity appears. This can clearly be seen in the inset of figure 5. These two $Q$-values are beyond the Bragg positions of the pure compounds AgCl and NaCl, respectively. Hence, the weak peaks cannot be due to phases with different lattice parameters. Rather, they may be regarded as satellites corresponding to the periodic concentration modulation. In this case, the distance from these satellites to the fundamental Bragg reflection ($\Delta Q \approx \pm 0.02$ r.l.u. $\approx 0.22$ nm$^{-1}$) is just given by the wavenumber of the modulation and should therefore coincide with $Q_{\max}$, the position of the correlation peak in the small-angle regime. In fact, comparison with the data of figure 4 yields a very good

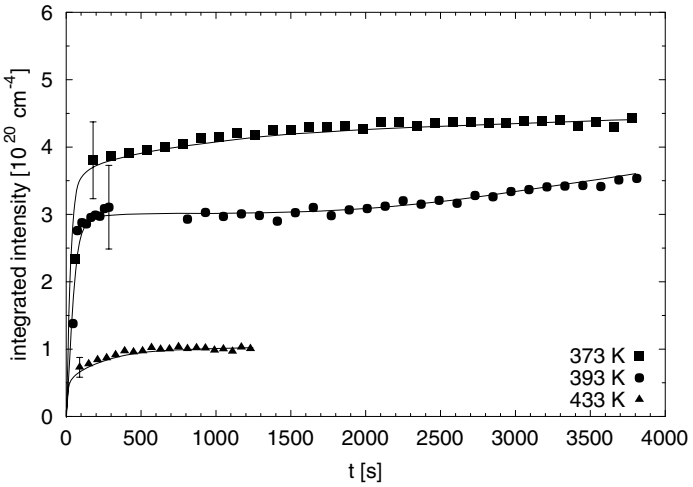


**Figure 4.** The time dependence of the integrated small-angle intensity for different temperatures. (The lines are drawn to guide the eye.).

agreement between these two independent experimental results. It should, however, be noted that the limitation of the statistics of the present data prevents further interpretation. Additional experiments, in particular on single crystals, are planned to elucidate this feature in more detail.

The lower part of figure 5 displays the Bragg profile obtained after more than 8 h. Even then, there is still a single peak which has become, however, considerably broader and slightly asymmetric. The centre of this peak is still fixed at the position corresponding to the lattice parameter of the homogeneous phase. Hence, the equilibrium state is still not reached.

## 4. Discussion

The SANS experiments below about 450 K exhibit the characteristic features of spinodal decomposition. The correlation peak reflects the presence of a collective composition wave which also gives rise to additional satellites in the diffraction pattern. Over the course of time this correlations peak is increasing and, simultaneously, it is shifted to smaller $Q$-values as displayed in figure 2. This coarsening effect is observed even at the earliest accessible times and is surprisingly well described by the law of Lifshitz and Slyozov [10]. This behaviour is different from that of the bromide system AgBr–NaBr, where an initial period was found in which $Q_{\max}$ is only slightly time dependent [1]. Hence, AgCl–NaCl is an example of a strongly non-linear system far beyond the applicability of the linearized models of Cahn and Hilliard [17] or Cahn, Hilliard and Cook [18] which predict the growth of concentration fluctuations at constant wavelength.

The time evolution of the SANS intensity as shown in figure 4 demonstrates that, similarly to in the bromide system, the chemical demixing takes place almost instantaneously and independently of temperature. The absolute values of the integrated intensity are, however, much lower than expected for complete decomposition: for a binary system consisting of well defined precipitates, the intensity can be calculated from the particle densities $n_i$, the compositions $x_i$ of the homogeneous (mixed) phase (index $m$) and the product phases (indices 1 and 2) and the respective densities of the scattering lengths $\rho_i$ as

$$4\pi \int_0^\infty \frac{\mathrm{d}\Sigma}{\mathrm{d}\Omega}(Q) Q^2 \,\mathrm{d}Q = (2\pi)^3 \left( \frac{n_1 x_1 - n_m x_m}{n_1 x_1 - n_2 x_2} \rho_2^2 + \frac{n_m x_m - n_2 x_2}{n_1 x_1 - n_2 x_2} \rho_1^2 - \rho_m^2 \right) \alpha \qquad (2)$$

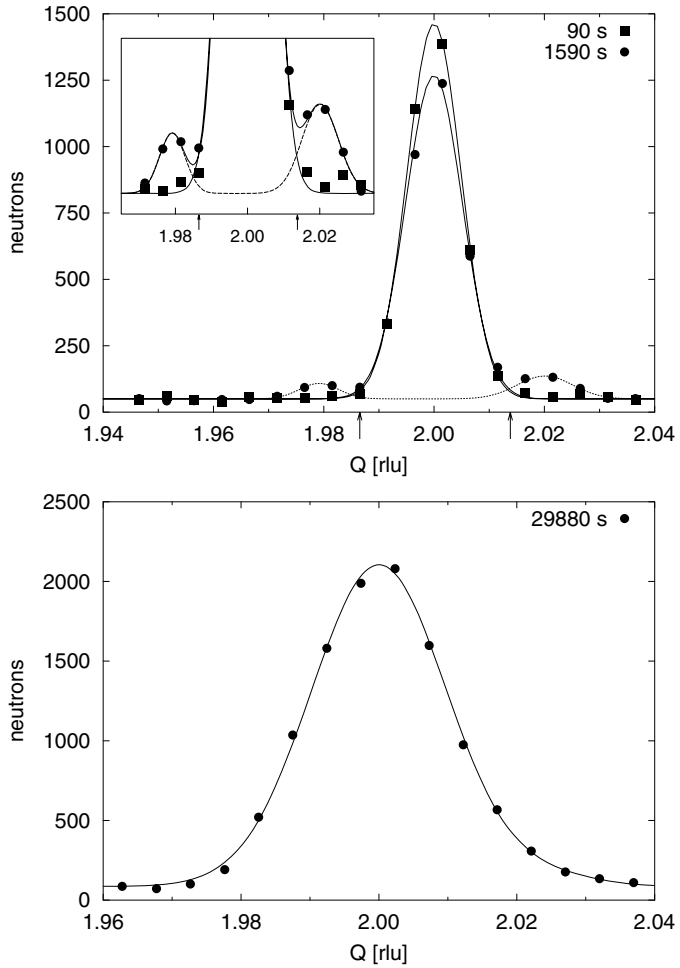


**Figure 5.** The time evolution of the (200) Bragg reflection at 373 K. Top: Bragg profiles after 90 s and 1590 s. The arrows label the positions where the Bragg peaks of the two equilibrium phases with binodal concentrations would be expected. The inset shows the appearance of satellites on an enlarged intensity scale. Bottom: the Bragg profile after 29 880 s.

where $\alpha$ is the degree of decomposition [1]. Here, it is assumed that the total volume is conserved during decomposition[3]. If the particle densities of the individual phases are identical ($n_1 = n_2 = n_m = n$), equation (2) reduces to the well known relation [19]

$$4\pi \int_0^\infty \frac{\mathrm{d}\Sigma}{\mathrm{d}\Omega}(Q) Q^2 \,\mathrm{d}Q = (2\pi)^3 (\rho_A - \rho_B)^2 (x_1 - x_m)(x_m - x_2)\alpha. \tag{3}$$

In stable equilibrium, equation (2) yields theoretical intensities of $18.5 \times 10^{20}$, $14.7 \times 10^{20}$ and $7.0 \times 10^{20}$ cm$^{-4}$ for the temperatures 373, 393 and 433 K, respectively, if the binodal compositions are used for $x_1$ and $x_2$. These values are considerably larger than the experimental data of figure 4.

[3] It can, in fact, be estimated from the lattice parameters of the pure phases that at 373 K (e.g.), the volume change during decomposition in the AgCl–NaCl system is far below 0.1%.

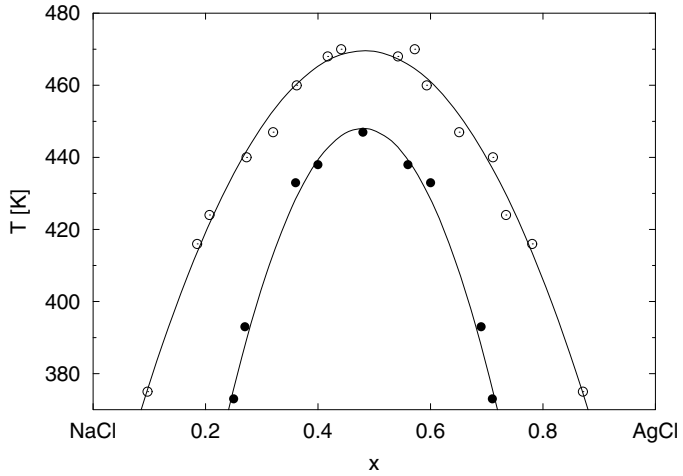


**Figure 6.** The equilibrium phase diagram (open symbols) after Sinistri *et al* [6] and the concentrations of the metastable states (closed symbols) as deduced from small-angle scattering.

Obviously, the process of demixing is stopped in an intermediate, metastable state. Either this state contains a large volume fraction of the homogeneous phase ($\alpha < 1$) or, which seems more reasonable, the concentrations of the product phases differ from the binodal ones.

The diffraction data prove that in these metastable states the lattice parameter is conserved, i.e. the particle density is unchanged. Hence, equation (3) can be used to calculate the respective concentrations of the metastable phases (for $\alpha = 1$ and under the assumption of an almost symmetrical miscibility gap). The results are shown in figure 8 along with the equilibrium data of Sinistri *et al* [6]. In this figure, the upper critical temperature of the spinodal, $T_s \approx 447 \pm 3$ K which is about 24 K below $T_{\mathrm{crit}}$, is also included. Similarly to in the analysis of the AgBr–NaBr data in [1], $T_s$ was determined as the highest temperature for which a correlation peak in the small-angle regime could be observed immediately after the quench. The lower curve, which is a polynomial fit to the data for the metastable states, can be regarded as the coherent spinodal.

The suppression $\Delta T$ of the spinodal is a consequence of coherency strains. According to Cahn [2], this temperature interval can be calculated from the elastic parameters as

$$\Delta T = T_{\mathrm{crit}} - T_s = 2\eta^2 \frac{E}{1-\nu} \frac{x_c\,(1-x_c)}{nk_B} \approx 20.6\ \mathrm{K} \tag{4}$$

when the relative difference of the lattice parameters $\eta = 0.017$, the Young modulus $E = 30.2$ GPa (taken as the average of the data for the pure substances at 447 K [20]), the Poisson ratio $\nu \approx 0.33$ and the particle density $n = 2.3 \times 10^{22}$ cm$^{-3}$ are used. Obviously, there is a very good agreement between experiment and calculation.

The diffraction data yield that there is no significant change of lattice parameter within the timescale of the present experiments. Hence, the decomposition process takes place within the frame of the fixed chloride sublattice until the compositions on the metastable coherent spinodal are reached. Since the sodium-rich (silver-rich) phase exhibits a smaller (larger) lattice parameter than in equilibrium, it is subjected to an internal compressive (tensile) stress. From the lattice parameters and the elastic modulus, the magnitude of these stresses can be estimated as 150 MPa.

Even after an ageing time of more than 8 h at 373 K, these stresses are not released. The single Bragg peak (figure 5) yields that the equilibrium state is still not reached. This is different

from the findings in the bromide system [1] where the mechanical relaxation was indeed observed to take place on a timescale of some 10 min at not-too-low temperatures. Hence, it is concluded that the driving force for the relaxation of the lattice is considerably reduced in the chloride system due to the smaller lattice parameter mismatch.

It should be noted that in the nucleation regime of the phase diagram, i.e. at temperatures between $T_{\mathrm{crit}}$ and $T_s$, the decomposition process is so sluggish that no significant effect on the Bragg reflections, similar to the results for the AgBr–NaBr system, could be observed within the timescale of the present experiments. This finding also implies that the diffraction results are not affected by the reduced quench rates as compared to the SANS experiments. All processes which lead to a significant change of the Bragg profiles take far more time than that needed to reach the ageing temperatures.

## 5. Conclusions

By the combination of time-resolved small-angle scattering and diffraction we were able to show that the decomposition process in AgCl–NaCl solid solutions below the spinodal temperature is governed by two different mechanisms. On the one hand, fast chemical demixing within the rigid framework of the anion sublattice can be described by the concept of spinodal decomposition. This process is hardly temperature dependent and leads to metastable intermediate states. On the other hand, the mechanical relaxation of the lattice and the adaptation of the equilibrium lattice parameters occur on a very much longer timescale. Hence, the splitting of structural Bragg reflections cannot be used to characterize the demixing process.

As demonstrated by Windgasse *et al* [21], the decomposition in ionic systems can be studied even in single crystals. Hence, more detailed information about the microscopic mechanism of phase separation can be obtained from time-resolved inelastic scattering from phonons, which directly reflect the evolution of interatomic interactions. Those investigations are currently under way and the results will be presented in the near future [22].

## Acknowledgments

Helpful discussions with P Elter and J Windgasse are gratefully acknowledged. Moreover, we are indebted to H Mitlacher (RWTH-Aachen and FZ Jülich) and R Thomas (FZ Jülich) for technical support during the data reduction.

## References

[1] Eckold G 2001 *J. Phys.: Condens. Matter* **13** 217
[2] Cahn J W 1961 *Acta Metall.* **9** 795
[3] Stokes R J and Li C H 1962 *Acta Metall.* **10** 535
[4] Hendricks R W, Baro R and Newkirk J B 1964 *Trans Metall. Soc. AIME* **230** 930
[5] Suslova V N, Shmidova N J, Zavadovskaya E K and Zvinchuk R A 1970 *Sov. Phys.–Dokl.* **15** 500
[6] Sinistri C, Riccardi R, Margheritis C and Tittarelli P 1971 *Z. Naturf.* a **27** 149
[7] Eckold G 1990 *Nucl. Instrum. Methods* A **289** 221
[8] Furukawa H 1984 *Physica* A **123** 497
[9] Porod G 1951 *Kolloid Z.* **124** 83
[10] Lifshitz I M and Slyozov V V 1961 *J. Phys. Chem. Solids* **19** 35
[11] Binder K and Stauffer D 1974 *Phys. Rev. Lett.* **33** 1006
[12] Binder K, Billotet C and Mirold P 1978 *Z. Phys.* **1330** 183
[13] Furukawa H 1981 *Phys. Rev.* A **23** 1535
[14] Binder K and Heermann D W 1985 *Scaling Phenomena in Disordered Systems* ed R Pynn and A Skjeltrop (New York: Plenum) p 207

[15] Heermann D W and Binder K 1987 *The Physics of Structure Formation* ed W Güttinger and G Dangelmayr (Berlin: Springer) p 42
[16] Li J 1995 *Nucl. Instrum. Methods* A **354** 164
[17] Cahn J W and Hilliard J E 1958 *J. Chem. Phys.* **28** 258
[18] Cook H E 1970 *Acta Metall.* **18** 297
[19] Gerold V 1961 *Phys. Status Solidi* **1** 37
[20] Every A G and McCurdy A K 1992 *Landolt–Börnstein New Series* vol 29, ed D F Nelson (Berlin: Springer) pp 76, 77, 240
[21] Windgasse J, Eckold G and Güthoff F 1997 *Physica* B **234–6** 153
[22] Caspary D, Elter P and Eckold G to be published